Longitudinal spin Seebeck effect in permalloy separated from the anomalous Nernst effect: Theory and experiment

J. Holanda,[1] O. Alves Santos,[1] R. O. Cunha,[2] J. B. S. Mendes,[3] R. L. Rodríguez-Suárez,[4] A. Azevedo,[1] and S. M. Rezende[1,*]

[1]*Departamento de Física, Universidade Federal de Pernambuco, 50670-901, Recife, Pernambuco, Brazil*

[2]*Centro Interdisciplinar de Ciências da Natureza, Universidade Federal da Integração Latino-Americana, 85867-970, Foz do Iguaçu, PR, Brazil*

[3]*Departamento de Física, Universidade Federal de Viçosa, 36570-900, Viçosa, MG, Brazil*

[4]*Facultad de Física, Pontifícia Universidad Católica de Chile, Casilla 306, Santiago, Chile*

(Received 31 March 2017; published 26 June 2017)

The longitudinal spin Seebeck effect (LSSE) consists in the generation of a spin current parallel to a temperature gradient in a magnetic material. The LSSE has only been measured unequivocally in magnetic insulators because in metallic films it is contaminated by the anomalous Nernst effect (ANE). Here we report theoretical and experimental studies of the LSSE in the metallic ferromagnet $N_{81}Fe_{19}$ (permalloy-Py) separated from the ANE. We have used trilayer samples of Py/NiO/NM (NM is a normal metal, Pt or Ta) under a temperature gradient perpendicular to the plane to generate a spin current in Py that is transported across the NiO layer and reaches the NM layer, where it is converted into a charge current by the inverse spin Hall effect. The LSSE is detected by a voltage signal in the NM layer while the ANE is measured by the voltage induced in the Py layer. The separation of the two effects is made possible because the antiferromagnetic insulator NiO layer transports spin current while providing electrical insulation between the Py and NM layers. The measured spin Seebeck coefficient for Py has a value similar to the one for the ferrimagnetic insulator yttrium iron garnet, with the same sign, and is in good agreement with the value calculated with a thermoelectric spin drift-diffusion model.

DOI: 10.1103/PhysRevB.95.214421

I. INTRODUCTION

The spin Seebeck effect refers to the generation of a spin current by a thermal gradient in a magnetic material, and is a magnetic analog of the thermoelectric Seebeck effect. The discovery in 2008 of the spin Seebeck effect (SSE) by Uchida, Saitoh, and co-workers [1] gave birth to a new area of spintronics, the spin caloritronics, that has attracted considerable attention for its scientific interest and potential applications in thermomagnetic devices [2–6]. The pioneering experiments of Ref. [1] were done with a thermal gradient applied along a film of the metallic ferromagnet $N_{81}Fe_{19}$, known as permalloy (Py), in the so-called transverse configuration. The effect was detected by the voltage signals measured along thin Pt strips deposited at the ends of the Py film, resulting from the conversion of the spin current into charge current by means of the inverse spin Hall effect (ISHE) [7–12]. Soon after the experiments with Py, Uchida, Saitoh, and co-workers demonstrated the existence of SSE in the longitudinal configuration (LSSE) in the ferrimagnetic insulator yttrium iron garnet (YIG) in contact with a thin Pt layer [13].

In the LSSE, one employs a bilayer made of a ferromagnetic insulator (FMI) with an attached metallic layer (ML). A temperature gradient $\nabla_\perp T$ applied perpendicularly to the plane of the FMI creates a spin current in the same direction that flows into the ML where it is partially converted by the ISHE into a charge current and detected by the associated voltage [2–6,13]. The electric field in the ML can be expressed in terms of the perpendicular temperature gradient in the form $\vec{E}_{\rm SSE} = -S_{\rm SV}\hat{\sigma} \times \nabla_\perp T$, where $S_{\rm SV}$ is often called the (voltage) spin-Seebeck coefficient and $\hat{\sigma}$ is the spin polarization determined by the direction of the applied magnetic field. In a bilayer made of a metallic ferromagnetic (FM) film and a normal metal layer under a thermal gradient applied perpendicularly to the plane, one also expects to have LSSE. However, in the FM film there is also an electric field created by the classical anomalous Nernst effect (ANE) $\vec{E}_{\rm ANE} = -\alpha_N \hat{\sigma} \times \nabla_\perp T$, where α_N is the anomalous Nernst coefficient [14–25]. The superposition of the voltages created by the two effects precludes the measurement of the LSSE so that it is generally accepted this effect cannot be observed in metallic ferromagnets, such as permalloy [2–6,13,20].

In this paper we demonstrate the existence of the longitudinal SSE in a film of metallic ferromagnetic permalloy where a spin current is created by a thermal gradient applied perpendicularly to the film plane. This was made possible by inserting a thin NiO layer between the NM and Py films. As recently discovered, NiO is an insulating room temperature antiferromagnet that blocks the flow of charge current but transports spin currents [26–33]. Thus one can measure the LSSE by means of the voltage generated in the NM layer by the spin-to-charge ISHE conversion and separately measure the ANE by the voltage induced in the Py layer. The paper is organized as follows. In Sec. II we describe the thermoelectric spin drift-diffusion model for the LSSE in a metallic ferromagnet and apply the results to permalloy. In Sec. III we describe the sample preparation and present the experimental measurements of the ANE and LSSE. Finally, in Sec. IV we discuss the results and compare the LSSE in Py with that in YIG.

II. THERMOELECTRIC SPIN DRIFT-DIFFUSION MODEL FOR THE LSSE IN METALLIC FERROMAGNETS

In this section we consider a simple bilayer made of a ferromagnetic metal (FM) in contact with a nonmagnetic

*Corresponding author: rezende@df.ufpe.br

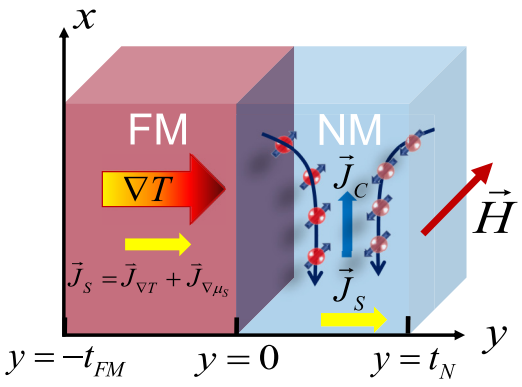

FIG. 1. Illustration of the ferromagnetic metal (FM)/metallic layer (ML) bilayer and coordinate axes used to formulate the theoretical model for the longitudinal spin Seebeck effect.

(NM) layer, under a temperature gradient normal to the plane and with a static magnetic field H applied in the plane, as illustrated in Fig. 1. We choose a coordinate system with the z axis parallel to the magnetic field H applied in the plane, and the y axis perpendicular to the plane, shown in Fig. 1. Our goal here is to calculate the spin current created by the thermal gradient in the FM and injected into the NM layer. As is well known, in a magnetic insulator, such as YIG, a spin current is carried by the collective spin excitations, spin waves, or magnons. In a metallic ferromagnet, such as Py, the spin current can be carried by the conduction electrons (electrons with opposite spins moving in opposite directions) and also by magnons. As shown in Refs. [34,35], under a thermal gradient the magnonic spin current is proportional to the magnon lifetime. Since in Py the magnon lifetime is typically two orders of magnitude smaller than in YIG, the magnonic contribution to the LSSE in Py is small and we consider here only the electronic thermoelectric transport. This has been treated in detail in Refs. [36,37] but with boundary conditions that are not appropriate for the structure in Fig. 1. For completeness we present here the full formulation of the thermoelectric spin current generation. For the FM layer in Fig. 1 we consider a homogeneous metallic ferromagnet in which the spin current is carried by electrons with spin denoted by $\sigma = \pm 1$, energy ε_k^σ, and momentum $\hbar\vec{k}$. In thermodynamic equilibrium at a temperature T, the electrons are distributed among the available states according to the Fermi-Dirac distribution function $f^\sigma(\vec{k},\vec{r}) = [e^{(\varepsilon_k^\sigma - \mu^\sigma)/k_B T} + 1]^{-1}$, where μ^σ is the spin-dependent chemical potential. In the presence of external fields, temperature gradient, and random scattering processes, the evolution of $f^\sigma(\vec{k},\vec{r})$ at a position $\vec{r}$ is governed by the Boltzmann transport equation (BTE). In steady state BTE reads

$$\left(\vec{v}_k \cdot \nabla_r + \frac{\vec{F}^\sigma}{\hbar} \cdot \nabla_k\right) f^\sigma(\vec{k},\vec{r}) = \left(\frac{\partial f^\sigma}{\partial t}\right)_{\text{scatt.}}, \quad (1)$$

where $\vec{v}_k = (1/\hbar)\nabla_k \varepsilon_k$ is the electron velocity and $\vec{F}^\sigma(\vec{r})$ is the external force on the electrons. The scattering term on the right-hand side contains spin-conserving and spin-flip impurity scattering that can be modeled, in the relaxation time approximation, by [36]

$$\left(\frac{\partial f^\sigma}{\partial t}\right)_{\text{scatt.}} = -\frac{[f^\sigma(\vec{k},\vec{r}) - f^\sigma(\varepsilon_k,\vec{r})]}{\tau^\sigma} - \frac{[f^\sigma(\varepsilon_k,\vec{r}) - f^{-\sigma}(\varepsilon_k,\vec{r})]}{\tau_{\text{sf}}}, \quad (2)$$

where $f^\sigma(\varepsilon_k,\vec{r}) = \int d\Omega_k f^\sigma(\vec{k},\vec{r})/4\pi$ is the momentum averaged electron distribution, τ^σ is the transport relaxation time, and τ_{sf} is the spin-flip relaxation time. Since $\tau^\sigma \ll \tau_{\text{sf}}$ momentum relaxation occurs first, followed by a slow spin relaxation. In the spirit of the linear response theory, we assume that the distribution function can be written as

$$f^\sigma(\vec{k},\vec{r}) \approx f_0(\varepsilon_k) + [g^\sigma(\vec{k},\vec{r}) + \mu^\sigma(\vec{r})]\left(-\frac{\partial f_0}{\partial \varepsilon_k}\right)_{\varepsilon_F}, \quad (3)$$

where with the introduction of the factor $(-\partial f_0/\partial\varepsilon_k)_{\varepsilon_F}$ we are explicitly recognizing that the transport involves only electrons with energy close to the Fermi energy ε_F. Introducing the spin-dependent effective electric field $\vec{E}^\sigma = \vec{E} + \nabla_r \mu^\sigma(\vec{r})/e$ (e is the electron charge), related to the force on the electrons $\vec{F}^\sigma = e\vec{E}^\sigma$, considering that $g^\sigma(\vec{k},\vec{r})$ varies slowly with momentum and in space, so that $\nabla_k g^\sigma(\vec{k},\vec{r}) \approx 0$, $\nabla_r g^\sigma(\vec{k},\vec{r}) \approx 0$, and that $\tau^\sigma \ll \tau_{\text{sf}}$, substitution of Eq. (3) into the BTE Eq. (1) leads to

$$g^\sigma(\vec{r},\vec{k}) = \tau^\sigma\, \vec{v}_k \cdot \frac{\partial \varepsilon_k}{\partial T} \nabla_r T - \frac{\hbar e \tau^\sigma}{m} \vec{k} \cdot \vec{E}^\sigma. \quad (4)$$

Thus Eq. (3) leads to

$$f^\sigma(\vec{k},\vec{r}) \approx f_0(\varepsilon_k) - \tau^\sigma \left(\frac{\partial f_0}{\partial T}\right) \vec{v}_k \cdot \nabla_r T + \frac{\hbar e \tau^\sigma}{m}\left(\frac{\partial f_0}{\partial \varepsilon_k}\right)_{\varepsilon_F} \vec{k} \cdot \vec{E}^\sigma - \mu^\sigma(\vec{r})\left(\frac{\partial f_0}{\partial \varepsilon_k}\right)_{\varepsilon_F}. \quad (5)$$

With this distribution function we can calculate various quantities of interest. We consider the electrons described by a simple Stoner model for a ferromagnetic metal, with energies $\varepsilon_k^\sigma = \varepsilon_k + \sigma\,\Delta$, where $\Delta(T)$ is the temperature dependent exchange splitting [36,38]. The charge current density with spin polarization σ is given by

$$\vec{J}_C^\sigma = \frac{e}{V} \sum_k f^\sigma(\vec{k},\vec{r})\, \vec{v}_k. \quad (6)$$

This is calculated taking into account that $\sum_{\vec{k}} f_0(\vec{k},\vec{r})\, \vec{v}_k = 0$ and $\sum_{\vec{k}} \vec{v}_k = 0$. The total charge current density is $\vec{J}_C = \vec{J}_C^\sigma + \vec{J}_C^{-\sigma}$ while the spin current density, in units of angular momentum, is $\vec{J}_S = \hbar/2e\,(\vec{J}_C^\sigma - \vec{J}_C^{-\sigma})$. Using Eq. (5) in Eq. (6), considering $\vec{E} = 0$, $\vec{J}_C = 0$, one can show that the spin current density with polarization in the field direction is the sum of two parts $\vec{J}_S = \vec{J}_{\nabla T} + \vec{J}_{\nabla \mu_S}$, where

$$\vec{J}_{\nabla T} = -\frac{\hbar}{(2\pi)^3} \int d^3k\, \tau \left(\frac{\partial f_0}{\partial \varepsilon_k}\right)_{\varepsilon_F} \frac{\partial \Delta}{\partial T}\, \vec{v}_k (\vec{v}_k \cdot \nabla_r T) \quad (7)$$

is the contribution from the thermally induced drift of electrons with temperature-dependent exchange splitting, and

$$\vec{J}_{\nabla \mu_S} = \frac{\hbar}{(2\pi)^3} \int d^3k\, \frac{\tau}{m} \left(\frac{\partial f_0}{\partial \varepsilon_k}\right)_{\varepsilon_F} \vec{v}_k (\vec{k} \cdot \nabla_r \mu_S) \quad (8)$$

is due to the spatial variation of the spin accumulation, defined by $\mu_S = (\mu^{\uparrow} - \mu^{\downarrow})/2$ [39,40]. In Eqs. (7) and (8), $\tau = (\tau^{\uparrow} + \tau^{\downarrow})/2$ and m is the electron mass. With the temperature gradient normal to the plane, Eq. (7) gives the spin current in the y direction

$$J_{\nabla T} = -S_S \frac{\partial T}{\partial y}, \tag{9}$$

$$S_S = \frac{\hbar}{(2\pi)^3} \int \tau \left(\frac{\partial f_0}{\partial \varepsilon_k}\right)_{\varepsilon_F} \frac{\partial \Delta}{\partial T} v_{ky}^2 \, d^3k. \tag{10}$$

The integral in Eq. (8) gives a factor proportional to the diffusion coefficient D_e, such that, with the Einstein relation $\sigma_c = e^2 D_e \, N(\varepsilon_F)$, where σ_c is the charge conductivity and $N(\varepsilon_F)$ the density of states at the Fermi energy, Eq. (8) becomes

$$J_{\nabla \mu_S} = -\frac{\hbar \sigma_c}{2e^2} \frac{\partial \mu_S}{\partial y}. \tag{11}$$

From Boltzmann equation one can also show [36,37,39,40] that the spin accumulation obeys a diffusion equation

$$\frac{\partial^2 \mu_S(y)}{\partial y^2} = \frac{\mu_S(y)}{\lambda_{\rm sf}^2}, \tag{12}$$

where $\lambda_{\rm sf}$ is the spin-flip diffusion length, related to the diffusion coefficient by $\lambda_{\rm sf} = \sqrt{D_e \, \tau_{\rm sf}}$. The solutions of Eq. (12) for the FM layer in the geometry of Fig. 1 are

$$\mu_S(y) = A \cosh[(y + t_{\rm FM})/\lambda_{\rm sf}] + B \sinh[(y + t_{\rm FM})/\lambda_{\rm sf}], \tag{13}$$

where A and B are coefficients to be determined by the boundary conditions. Using Eq. (13) in Eq. (11) one obtains the total y component of the spin-current density in the FM layer

$$J_S(y) = -S_S \nabla_y T - \frac{\hbar \sigma_c}{2e^2 \lambda_{sf}} A \sinh[(y + t_{\rm FM})/\lambda_{\rm sf}] - \frac{\hbar \sigma_c}{2e^2 \lambda_{\rm sf}} B \cosh[(y + t_{\rm FM})/\lambda_{\rm sf}], \tag{14}$$

where the coefficients A and B are be determined by the boundary conditions at $y = -t_{\rm FM}$ and $y = 0$. The boundary conditions are defined by conservation of the angular momentum flow that requires continuity of the spin currents at the interfaces. Using the boundary condition $J_S(y = -t_{\rm FM}) = 0$ at the substrate/FM interface we obtain with Eqs. (13) and (14):

$$J_S(0^-) = -S_S \nabla_y T \left[\frac{\cosh(t_{\rm FM}/\lambda_{\rm sf}) - 1}{\cosh(t_{\rm FM}/\lambda_{\rm sf})}\right] - \mu_S(0) \frac{\hbar \sigma_c}{2e^2 \lambda_{\rm sf}} \tanh(t_{\rm FM}/\lambda_{\rm sf}). \tag{15}$$

The spin current created by the thermal gradient in the FM flows through the FM/NM interface and produces in the NM layer a spin accumulation with the associated spin current that at $y = 0^+$ is given by [39,40]

$$J_S(0^+) = \frac{g_{\rm eff}^{\uparrow\downarrow}}{4\pi} \mu_S(0^-), \tag{16}$$

where $g_{\rm eff}^{\uparrow\downarrow}$ is the real part of the effective spin mixing conductance that takes into account the spin-pumped and backflow spin currents [39,40]. Using Eqs. (15) and (16) in the boundary condition at the FM/NM interface $J_S(0^-) = J_S(0^+)$, and considering $\hbar \sigma_c / 2e^2 \lambda_{\rm sf} \gg g_{\rm eff}^{\uparrow\downarrow}/4\pi$, we obtain the spin current in the NM due to the LSSE

$$J_S(0^+) = -C_S \, \rho(t_{\rm FM}/\lambda_{\rm sf}) \, \partial_y T, \tag{17}$$

where ρ is a factor that represents the effect of the finite FM layer thickness, given by

$$\rho = \frac{\cosh(t_{\rm FM}/\lambda_{\rm sf}) - 1}{\sinh(t_{\rm FM}/\lambda_{\rm sf})}, \tag{18}$$

and $C_S = S_S \, g_{\rm eff}^{\uparrow\downarrow} e^2 \lambda_{\rm sf} / 2\pi \hbar \sigma_c$. With some approximations one can obtain a simple expression for C_S. Considering in Eq. (9) a parabolic energy band for the electrons, using $(\partial f_0/\partial \varepsilon_k)_{\varepsilon_F} \approx -\delta(\varepsilon - \varepsilon_F)$ and the Drude model for the conductivity $\sigma_c = n_e \, e^2 \tau / m$, where n_e is the electron concentration, we obtain

$$C_S = \frac{g_{\rm eff}^{\uparrow\downarrow} \, \lambda_{sf}}{3\pi \, n_e} (-\partial \Delta / \partial T) \, N(\varepsilon_F) \, \varepsilon_F. \tag{19}$$

Notice that Eqs. (17) and (18) have the same form as the one for the LSSE in a FMI/NM bilayer [34,35]. This is so because in the thermoelectric model the spin current created by the thermal gradient is carried by the spin accumulation, while in the bulk magnon model for the FMI it is carried by the magnon accumulation, and in both cases the evolution is governed by the Boltzmann transport equation and the diffusion equation, subject to the same boundary conditions.

The spin accumulation in the NM obeys a diffusion equation like Eq. (12) with a spin-flip diffusion length λ_N [39,40]. With the boundary condition at the surface of the NM layer $J_S(y = t_N) = 0$, one finds the spin accumulation and the spin current for $0 \leqslant y \leqslant t_N$. The spin current is given by

$$J_S(y) = J_S(0^+) \frac{\sinh[(t_N - y)/\lambda_N]}{\sinh(t_N/\lambda_N)}. \tag{20}$$

Due to the inverse spin Hall effect, the spin-current density $\vec{J}_S$ flowing into the NM layer generates a charge-current density given by $\vec{J}_C = \theta_{\rm SH}(2e/\hbar) \, \vec{J}_S \times \hat{\sigma}$, where $\theta_{\rm SH}$ is the spin-Hall angle and $\hat{\sigma}$ is the spin polarization. With the magnetic field in the plane and transverse to the long direction of the NM layer, the resulting charge current produces a dc ISHE voltage at the ends of the NM layer. Since the spin current at the FM/NM interface diffuses into the NM layer with diffusion length λ_N, in order to calculate the voltage at the ends of the NM layer one has to integrate the charge-current density along x and y so that the SSE-ISHE voltage becomes

$$V_{\rm SSE} = R_N \, w \lambda_N \frac{2e}{\hbar} \theta_{\rm SH} \tanh\left(\frac{t_N}{2\lambda_N}\right) J_S(0) \cos\phi, \tag{21}$$

where R_N, t_N, and w are the resistance, thickness, and width of the NM layer, respectively, and ϕ is the angle of the spin polarization determined by the direction of the magnetic field as in Fig. 3(a). Finally, with Eqs. (19) and (21) we can write the charge current $I_{\rm SSE} = V_{\rm SSE}/R_N$ produced by the temperature gradient, for $\phi = 0$, as

$$I_{\rm SSE} = -S_{\rm SSE} \, \rho \, \partial_y T, \tag{22}$$

where

$$S_{\mathrm{SSE}}=\frac{2\,g_{\mathrm{eff}}^{\uparrow\downarrow}\,\lambda_{\mathrm{sf}} w\,\lambda_N e\theta_{\mathrm{SH}}}{3\pi\, n_e\,\hbar}\,\tanh(t_N/2\lambda_N)\,(-\partial\Delta/\partial T)\,N(\varepsilon_F)\,\varepsilon_F \tag{23}$$

is the spin Seebeck coefficient for LSSE in a metallic ferromagnet. Note that often the spin Seebeck coefficient is defined with reference to the voltage measured in the NM layer. One disadvantage of using the voltage is that it varies with the resistance, so that two samples made with the same materials but with different NM layer thicknesses would have different spin Seebeck voltage coefficients.

III. EXPERIMENTS

The voltage produced by the LSSE in a FM/NM bilayer adds to the one created by the anomalous Nernst effect. Previous studies of the longitudinal spin-Seebeck effect in Py/NM do not distinguish the voltages generated by the two effects [41–43]. Here we report experiments in which the two effects are separated by the use of a thin NiO layer between the Py and NM layers. The sample structures used to measure the LSSE and ANE in Py are shown schematically in Figs. 2(a) and 3(a). The samples consist of a Py layer deposited by dc magnetron sputtering on a Si(0.4 mm)/SiO(300 nm) substrate with lateral dimensions 9 mm × 2.5 mm. Samples with several Py film thicknesses were prepared in order to measure the thickness dependencies of the effects. For the initial measurement of the voltage due only to the ANE we used a single Py film, with no capping layer, as in Fig. 2(a). For measuring the ANE and LSSE voltages separately we use the structure in Fig. 3(a), where a 5 nm thick NiO layer was deposited onto the Py layer by rf magnetron sputtering at 160 °C leaving 0.5 mm clearances at the ends for the electrodes. Then a Pt or Ta films, with thickness 6 nm, were sputter deposited on the central part of the NiO layer using a shadow mask to make a film with smaller width to avoid contact with the Py layer. Finally, Ag electrodes were attached to the ends of the Py, Pt, and Ta layers, as shown in Figs. 2(a) and 3(a), for measuring the voltages directly with a nanovoltmeter. The distances between the electrodes are 8 mm in the Py layer and 5 mm in the Pt and Ta layers. The resistances measured between the electrodes vary from 85 to 95 Ω in Pt, it is 120 Ω in Ta, while in Py it varies inversely with the thickness, as shown in the inset of Fig. 6(b). The resistances measured between the contacts in the NM and Py layers are above 50 MΩ, indicating that the NiO layer provides electrical insulation between them. A commercial Peltier module, of width 4 mm, was used to heat or cool the side of the Pt (Ta) layer while the substrate was maintained in thermal contact with a copper block at room temperature. The temperature difference ΔT across the sample is measured with a differential thermocouple.

Figure 2(b) shows the ANE voltage versus magnetic field measured in the Py layer with thickness 30 nm, for several values of the temperature difference ΔT, all with the Peltier

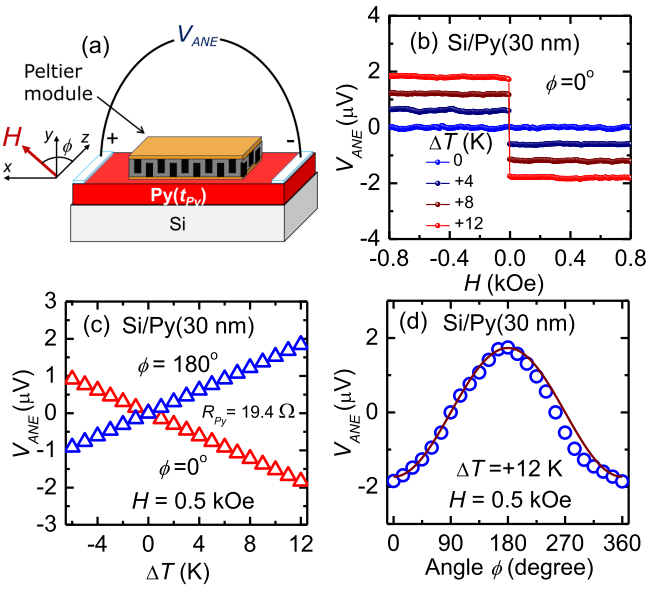

FIG. 2. (a) Schematic illustration of the Py sample used to measure the voltage generated by the anomalous Nernst effect (ANE). All measurements shown in the figure were done with Py layer thickness of 30 nm. (b) Variation with magnetic field of the ANE voltage measured in the Py layer with four values of the temperature difference ΔT indicated. Positive ΔT corresponds to the Peltier module warmer than the Si substrate. (c) ANE voltage versus temperature difference measured with $H = 0.5$ kOe in two field directions. (d) Variation of the ANE voltage with the magnetic field angle ϕ measured with $H = 0.5$ kOe and $\Delta T = +12$ K. Solid curve is a fit with $A\cos\phi$.

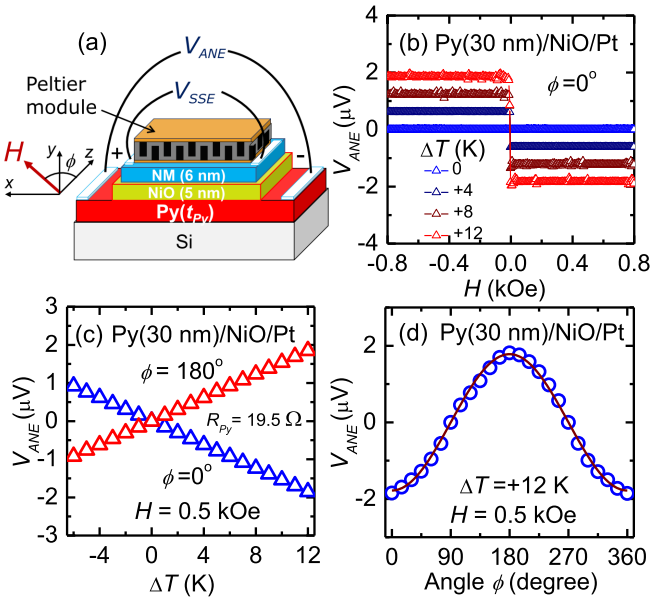

FIG. 3. (a) Schematic illustration of the Py sample structure used to measure the voltages generated in Si/Py/NiO/Pt by the ANE and LSSE. All measurements shown in the figure were done in the sample with Py layer thickness of 30 nm. (b) Variation with magnetic field of the ANE voltage measured in the Py layer with four values of the temperature difference ΔT indicated. Positive ΔT corresponds to the Pt layer warmer than Py. (c) ANE voltage versus temperature difference measured with $H = 0.5$ kOe in two field directions. (d) Variation of the ANE voltage with the magnetic field angle ϕ measured with $H = 0.5$ kOe and $\Delta T = +12$ K. Solid curve is a fit with $A\cos\phi$.

module warmer than the Si substrate ($\Delta T > 0$). The data have the shape of the hysteresis curve of Py with very small coercitivity in the field scale of the measurements. The change in sign of the ANE voltage with field reversal is due to the change in the polarization. Figure 2(c) shows the ANE voltage as a function of the temperature difference ΔT measured with a field of $H = 0.5$ kOe in two opposite directions. Note that the resistance of the Py layer, shown in the figure, is the one corresponding to the length of the Peltier element, which is 1/2 the value measured between the electrodes. Figure 2(d) shows the field angle dependence of the ANE voltage measured with $H = 0.5$ kOe and $\Delta T = +12$ K. Figure 3 shows the ANE voltage measured in the Py layer of the trilayer sample Py(30 nm)/NiO(5 nm)/Pt(6 nm). The data of Figs. 2 and 3 are almost identical, demonstrating that the voltage measurements in the Py layer of the trilayer samples correspond to the anomalous Nernst effect, with no interference of the insulating NiO layer.

The data of Figs. 2 and 3 show that, as expected from the equation for the ANE, $\vec{E}_{\rm ANE} = -\alpha_N\, \hat{\sigma} \times \nabla_\perp T$, the voltage varies linearly with temperature and changes sign with the field reversal. Figures 2(d) and 3(d) show that the angle dependence of the voltage is described by the function $\cos\phi$, as predicted by the vector product in the ANE equation. From the data we can obtain the anomalous Nernst coefficient using the relation $\alpha_N = V_{\rm ANE}\, t_{\rm Py}/(L\, \Delta T_{\rm Py})$, where L is the length of the Py film under the Peltier module, $t_{\rm Py}$ is the film thickness, and $\Delta T_{\rm Py}$ is the temperature difference across the film, with the sign as defined before. The temperature difference across the Py film is related to the one measured across the sample by $\Delta T_{\rm Py} \approx (t_{\rm Py}\, K_{\rm Si}/t_{\rm Si}\, K_{\rm Py})\Delta T$, where $K_{\rm Py}$ and $K_{\rm Si}$ are the thermal conductivities of Py and Si, so that $\alpha_N = V_{\rm ANE}\, t_{\rm Si}\, K_{\rm Py}/(L\, K_{\rm Si}\Delta T)$. Using the values $\Delta T = +12$ K, $V_{\rm ANE} = 1.85\,\mu$V, $L = 4$ mm, $t_{\rm Si} = 0.4$ mm, $K_{\rm Si} = 148$ W/(K m), $K_{\rm Py} = 46.4$ W/(K m) [44,45], we obtain $\alpha_N = 4.8$ nV/K, which is similar to values measured by other authors [19].

In the Py/NiO/NM trilayer, the temperature gradient across the Py layer has two effects: One is to generate a voltage in the plane by the ANE, as demonstrated by the data in Figs. 2 and 3, the other is to produce a spin current by the longitudinal spin Seebeck effect, as presented in Sec. II, that is transported through the NiO layer and is detected in the NM layer as an electric voltage resulting from the spin-to charge conversion by the ISHE. As shown in Ref. [33], the spin current density $J_S(0)$ produced by the LSSE is injected in the Py/NiO interface, is transported through the NiO layer (thickness t) by the diffusion of antiferromagnetic magnons, and reaches the interface at $y = t$ with a value proportional to $J_S(0)$, given by $J_S(t) = F_t\, J_S(0)$, where

$$F_t = c\,[\sinh(t/l_m) + c\,\cosh(t/l_m)]^{-1}, \qquad (24)$$

where $c = g^{\uparrow\downarrow}_{\rm 2eff} b\, l_m/D_m$ is a dimensionless parameter proportional to the spin-mixing conductance of the interface at $y = t$, D_m and l_m are the diffusion constant and length of the magnon accumulation in NiO, and b is a factor involving integrations over the first Brillouin zone. The spin current $\vec{J}_S(t)$ reaching the NM layer produces a charge current with density given by $\vec{J}_C = \theta_{\rm SH}\, \vec{J}_S(t) \times \hat{\sigma}$, where $\theta_{\rm SH}$ is the spin Hall angle, so that

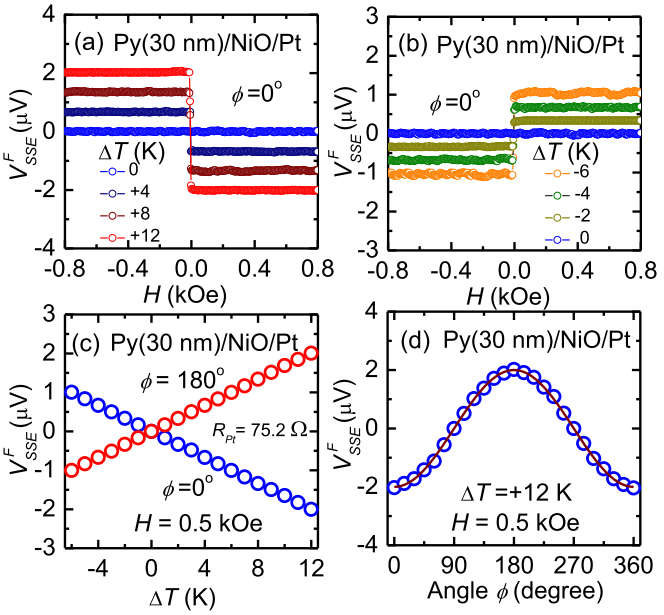

FIG. 4. (a) and (b) Variation with magnetic field of the dc ISHE-SSE voltage measured in the Pt layer created by the spin Seebeck effect in the Py layer for four values of ΔT as indicated. (c) Variation with temperature difference of the SSE voltage in the Pt layer measured with $H = 0.5$ kOe in two field directions. (d) Variation of the SSE voltage with the magnetic field angle ϕ measured with $H = 0.5$ kOe and $\Delta T = +12$ K. Solid curve is a fit with $A\cos\phi$.

the voltage measured in the NM layer corresponds to the spin current due to the LSSE in the Py layer reduced by the factor F_t which we denote by $V^F_{\rm SSE} = F_t\, V_{\rm SSE}$.

The LSSE in Py is demonstrated by the data in Figs. 4 and 5. Figures 4(a) and 4(b) show the voltage versus magnetic field measured in the Pt layer of the Py(30 nm)/NiO(5 nm)/Pt(6 nm) sample, for several values of the temperature difference ΔT. This voltage is produced by the charge current resulting from the ISHE conversion of the spin current generated by the thermal gradient across the Py film that is injected into the Py/NiO interface and transported across the NiO layer. Figure 4(c) shows the SSE voltage $V^F_{\rm SSE}$ as a function of the temperature difference ΔT measured with a field of $H = 0.5$ kOe in two opposite directions. As expected from the equation for the SSE, the voltage varies linearly with temperature and changes sign with the field reversal. Figure 4(d) shows the voltage measured with $H = 0.5$ kOe and $\Delta T = +12$ K as a function of the in-plane field angle, showing the $\cos\phi$ dependence expected from the cross product $\vec{J}_S \times \hat{\sigma}$. In regard to the sign of the spin current produced by the LSSE in the Py layer, we note that for the field in the $+z$ direction, a positive temperature gradient in the $+y$ direction creates a charge current in the $-x$ direction (negative voltage). Since the spin Hall angle of platinum is positive, the spin current is in the $-y$ direction, which is the same as observed in the LSSE in YIG/Pt bilayers [46,47]. In order to confirm the origin of the voltage in the NM layer, we have made measurements in a trilayer sample using Ta instead of Pt for the NM material, since it is known that it has a negative spin Hall angle [10,12]. Figure 5 shows voltage measurements

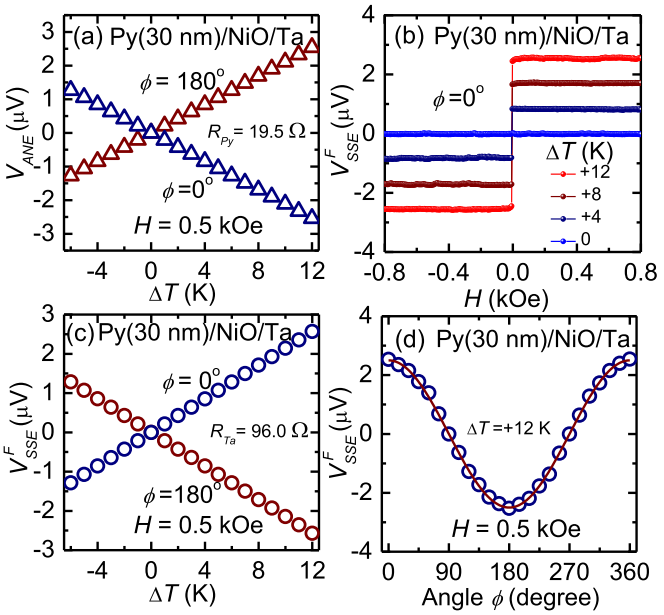

FIG. 5. (a) Variation with temperature difference of the ANE voltage measured in the Py layer in the trilayer sample Py(30 nm)/NiO(5 nm)/Ta(6 nm) with $H = 0.5$ kOe in two field directions. (b) Variation with magnetic field of the SSE voltage measured in the Ta layer created by the spin Seebeck effect in the Py layer for four values of ΔT as indicated. (c) Variation with temperature difference of the SSE voltage in the Ta layer measured with $H = 0.5$ kOe in two field directions. (d) Variation of the SSE voltage with the field angle ϕ measured with $H = 0.5$ kOe and $\Delta T = +12$ K. Solid curve is a fit with $A \cos\phi$.

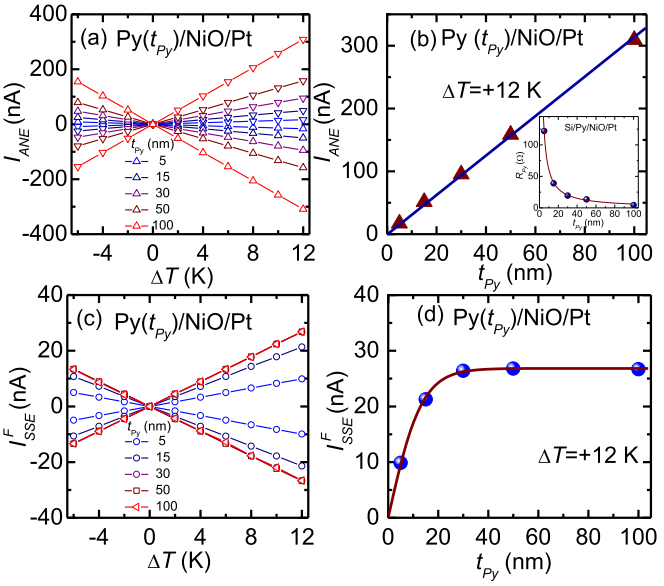

FIG. 6. (a) ANE current versus temperature difference measured in five samples of Py/NiO/Pt with varying Py thickness, with $H = 0.5$ kOe in two field directions. (b) Symbols represent the variation with Py layer thickness of the ANE current measured with $\Delta T = +12$ K while the solid line is a fit with a linear dependence. The inset shows the measured resistance of the Py layers and a fit with C/t_{Py}. (c) SSE current versus temperature difference measured in the same five samples with $H = 0.5$ kOe in two field directions. (d) Symbols represent the variation with Py layer thickness of SSE current measured with $\Delta T = +12$ K while the solid line is a fit with the thickness factor $\rho(t_{Py})$.

made in the Py(30 nm)/NiO(5 nm)/Ta(6 nm) trilayer sample. Figure 5(a) shows the voltage in the Py layer as a function of the temperature difference ΔT, measured with a field of $H = 0.5$ kOe in two opposite directions. The measured values are very similar to those in Figs. 2(c) and 3(c), in sign and magnitude, showing that the origin of the voltage is in the anomalous Nernst effect. However, the data in Figs. 5(b), 5(c), and 5(d) show signs that are opposite to those measured in the Py(30 nm)/NiO(5 nm)/Pt(6 nm) sample, consistent with the conversion by the ISHE in Ta with negative spin Hall angle, of a spin current produced in the LSSE in Py. Note that the amplitude of the voltages in Ta is 1.3 times the ones measured in Pt. This value is approximately the same as the ratio of the two resistances, which is consistent with the fact the spin Hall angles in Ta and Pt are similar in amplitude [10].

Another confirmation of the separation of the longitudinal spin Seebeck effect in Py from the anomalous Nernst effect is provided by measurements of the ANE and SSE voltages in samples with varying thickness of the Py film. This was carried out in samples with a single Py film and with Py/NiO/Pt trilayers. Figure 6(a) shows the ANE charge currents, obtained by dividing the measured voltages by the resistances of the Py layers in the length of the Peltier element (4 mm), as a function of ΔT, for $H = \pm 0.5$ kOe. The variation of the measured current with the Py film thickness is shown in Fig. 6(b) for $\Delta T = +12$ K. Similar measurements made in single Py films exhibit almost identical results. The measured linear dependence of the ANE current on the Py thickness is explained by the fact that the charge current density is $J_{\rm ANE} = \sigma_{\rm Py}\, E_{\rm ANE}$, where $\sigma_{\rm Py}$ is the electric conductivity of Py. Since α_N does not vary with the Py thickness, the ANE charge current $I_{\rm ANE} = w\, t_{\rm Py}\, J_{\rm ANE}$ is proportional to the Py thickness, as demonstrated in Fig. 6(b).

Figures 6(c) and 6(d) show that the dependence of the SSE current on the Py thickness is very different from the ANE and is qualitatively similar to the SSE measured in the insulating ferrimagnet yttrium iron garnet (YIG), a standard material used in studies of the longitudinal spin Seebeck effect (LSSE) [34,35,46–48]. Figure 6(d) shows a solid curve representing the best fit to data of the expression $I^F_{\rm SSE} = A\, \rho(t_{\rm Py})$, where $\rho(t_{\rm Py})$ is the thickness factor given by Eq. (18). The least-square deviation fit to the measurements with $\Delta T = +12$ K gives $A = 26.8$ nA and $l_{\rm sf} = 6.7$ nm. The good fit of theory to data represents another confirmation of the LSSE origin of the spin current detected in the Pt layer.

IV. INTERPRETATION AND DISCUSSION

Initially we use the data of Fig. 4 to compare the values of the spin-Seebeck coefficients of Py/Pt with that of the reference system YIG/Pt. Measurements similar to those in Figs. 4 and 5, done in a GGG/YIG(6 μm)/Pt(6 nm) bilayer as in Refs. [34,35,47], with $\Delta T = +6$ K gives a voltage of $V_{\rm SSE} = 2.2\,\mu$V. With the resistance of 75.2 Ω of the Pt layer in the length of the Peltier module (4 mm), this corresponds to a current $I_{\rm SSE} = 29.2$ nA. Since the Pt layer is very thin

and the thermal conductivities of YIG and GGG are almost the same, the temperature gradient across the YIG film is equal to the one across the GGG/YIG/Pt structure, $\nabla T_\perp = \Delta T/d$, where $d = 0.5\,\text{mm}$ is the thickness of the sample. From the SSE current measured in YIG/Pt we calculate the spin-Seebeck coefficient with $S_{S-\text{YIG/Pt}} = I_{\text{SSE}}\, d/\Delta T$, which gives $S_{S-\text{YIG/Pt}} = 0.24\,\text{nA cm/K}$. The calculation of the SSE coefficient for Py requires that we first consider the effect of the NiO layer, as explained earlier. From spin pumping measurements in samples with three different NiO layer thicknesses t_{NiO} and fit with the theoretical expression of Ref. [33], extrapolation to $t_{\text{NiO}} = 0$ shows that the spin current in the Py/NiO interface is 3.1 times the one reaching the Pt layer. Thus, from the data of Fig. 6(d), we infer the SSE current of Py/Pt bilayer for $\Delta T = +6\,\text{K}$, $I_{\text{SSE}} = 3.1 \times 26.8 = 83.1\,\text{nA}$. As argued earlier, the temperature difference across the Py film is related to the one measured across the sample by $\Delta T_{\text{Py}} \approx (t_{\text{Py}}\, K_{\text{Si}}/t_{\text{Si}}\, K_{\text{Py}})\Delta T$, so that $S_{S-\text{Py/Pt}} = I_{\text{SSE}}\, t_{\text{Si}}\, (K_{\text{Py}}/\, K_{\text{Si}})/\Delta T$. Using the values $\Delta T = +6\,\text{K}$, $I_{\text{SSE}} = 83.1\,\mu\text{V}$, $t_{\text{Si}} = 0.4\,\text{mm}$, $K_{\text{Si}} = 148\,\text{W/(K m)}$, and $K_{\text{Py}} = 46.4\,\text{W/(K m)}$, we obtain $S_{S-\text{Py/Pt}} = 0.22\,\text{nA cm/K}$, which is quite close to the value for YIG/Pt.

We now compare the measured spin Seebeck coefficient for Py/Pt with the value calculated with the thermoelectric spin diffusion model, given by Eq. (23). Use the following parameters for permalloy: $\lambda_{\text{sf}} = 6.7\,\text{nm}$ (measured here); Fermi energy $\varepsilon_F = 1.44 \times 10^{-11}\,\text{erg}$ [49]; free electron concentration $n_e = 2.75 \times 10^{23}\,\text{cm}^{-3}$ [50]; exchange splitting energy $\Delta(T = 0) = 2.16 \times 10^{-13}\,\text{erg}$ [51]. We consider a parabolic energy band so that the density of states can be calculated with $N(\varepsilon_F) = (1/2\pi)^2\,(2m/\hbar)^{3/2}\varepsilon_F^{1/2}$, from which we obtain $N(\varepsilon_F) = 6.44 \times 10^{33}\,\text{g}^{3/2}\,\text{erg}^{-5/2}\,\text{s}^{-3}$. We also consider that the exchange splitting $\Delta(T)$ is proportional to the magnetization $M(T)$ [38,52] and that $M(0) - M(T) = c_M\, T^{3/2} M(0)$ [52]. Using the measured $M(T)$ [53] we obtain $\partial\Delta(T)/\partial T = -8.13 \times 10^{-17}\,\text{erg/K}$. Using for platinum [10] $\lambda_N = 3.7\,\text{nm}$, $\theta_{\text{SH}} = 0.05$, $t_N = 6\,\text{nm}$, $w = 0.015\,\text{cm}$ and using for the spin mixing conductance $g_{\text{eff}}^{\uparrow\downarrow} = (3 \pm 2) \times 10^{14}\,\text{cm}^{-2}$, we obtain with Eq. (23) the spin Seebeck coefficient $S_{\text{SSE}} = 0.33 \pm 0.23\,\text{nA cm/K}$. The value measured experimentally, $S_{\text{S-Py/Pt}} = 0.22\,\text{nA cm/K}$, falls within this range, demonstrating very good agreement between theory and experiments.

In summary, we have demonstrated that it is possible to observe and measure the spin Seebeck effect in the longitudinal configuration (LSSE) in the metallic ferromagnet $N_{81}Fe_{19}$ (permalloy-Py) separated from the anomalous Nernst effect (ANE). By using trilayer samples of Py/NiO/Pt under a perpendicular temperature gradient, one can generate a spin current in Py that is transported through the NiO layer into the Pt layer where it is converted into a charge current by the inverse spin Hall effect. The ISHE was detected by a voltage signal in the Pt layer while the ANE was measured by the voltage induced in the Py layer. The use of the antiferromagnetic insulator NiO layer provides electrical insulation between the Py and Pt layers while maintaining spin current contact making possible the separation of the two effects. The measured spin Seebeck coefficient for Py has a value similar to the one for the ferrimagnetic insulator yttrium iron garnet, with the same sign, and is in good agreement with the value calculated with a thermoelectric spin drift-diffusion model.

ACKNOWLEDGMENTS

This research was supported in Brazil by Conselho Nacional de Desenvolvimento Científico e Tecnológico (CNPq), Coordenação de Aperfeiçoamento de Pessoal de Nível Superior (CAPES), Financiadora de Estudos e Projetos (FINEP), Fundação de Amparo à Pesquisa do Estado de Minas Gerais (FAPEMIG), and Fundação de Amparo à Ciência e Tecnologia do Estado de Pernambuco (FACEPE), and in Chile by Fondo Nacional de Desarrollo Científico y Tecnológico (FONDECYT) No. 1170723.

[1] K. Uchida, S. Takahashi, K. Harii, J. Ieda, W. Koshibae, K. Ando, S. Maekawa, and E. Saitoh, Nature (London) **455**, 778 (2008).
[2] G. E. W. Bauer, E. Saitoh, and B. J. van Wees, Nat. Mater. **11**, 391 (2012).
[3] H. Adachi, K. Uchida, E. Saitoh, and S. Maekawa, Rep. Prog. Phys. **76**, 036501 (2013).
[4] S. R. Boona, R. C. Myers, and J. P. Heremans, Energy Environ. Sci. **7**, 885 (2014).
[5] K. Uchida, H. Adachi, T. Kikkawa, A. Kirihara, M. Ishida, S. Yorozu, S. Maekawa, and E. Saitoh, Proc. IEEE **104**, 1946 (2016).
[6] H. Yu, S. D. Brechet, and J.-P. Ansermet, Phys. Lett. A **381**, 825 (2017).
[7] J. E. Hirsch, Phys. Rev. Lett. **83**, 1834 (1999).
[8] A. Azevedo, L. H. Vilela-Leão, R. L. Rodríguez-Suárez, A. B. Oliveira, and S. M. Rezende, J. Appl. Phys. **97**, 10C715 (2005).
[9] E. Saitoh, M. Ueda, H. Miyajima, and G. Tatara, Appl. Phys. Lett. **88**, 182509 (2006).
[10] A. Hoffmann, IEEE Trans. Mag. **49**, 5172 (2013).
[11] S. Maekawa, H. A. Adachi, K. Uchida, J. Ieda, and E. Saitoh, J. Phys. Soc. Jpn. **82**, 102002 (2013).
[12] J. Sinova, S. O. Valenzuela, J. Wunderlich, C. H. Back, and T. Jungwirth, Rev. Mod. Phys. **87**, 1213 (2015).
[13] K. Uchida, H. Adachi, T. Ota, H. Nakayama, S. Maekawa, and E. Saitoh, Appl. Phys. Lett. **97**, 172505 (2010).
[14] S. Y. Huang, W. G. Wang, S. F. Lee, J. Kwo, and C. L. Chien, Phys. Rev. Lett. **107**, 216604 (2011).
[15] A. Slachter, F. L. Bakker, and B. J. van Wees, Phys. Rev. B **84**, 020412(R) (2011).
[16] A. D. Avery, M. R. Pufall, and B. L. Zink, Phys. Rev. Lett. **109**, 196602 (2012).
[17] S. L. Yin, Q. Mao, Q. Y. Meng, D. Li, and H. W. Zhao, Phys. Rev. B **88**, 064410 (2013).
[18] D. Meier, D. Reinhardt, M. Schmid, C. H. Back, J.-M. Schmalhorst, T. Kuschel, and G. Reiss, Phys. Rev. B **88**, 184425 (2013).
[19] B. F. Miao, S. Y. Huang, D. Qu, and C. L. Chien, Phys. Rev. Lett. **111**, 066602 (2013).

[20] K. Uchida, M. Ishida, T. Kikkawa, A. Kirihara, T. Murakami, and E. Saitoh, J. Phys.: Condens. Matter **26**, 343202 (2014).
[21] D. Tian, Y. Li, D. Qu, X. Jin, and C. L. Chien, Appl. Phys. Lett. **106**, 212407 (2015).
[22] C. Fang, C. H. Wan, Z. H. Yuan, L. Huang, X. Zhang, H. Wu, Q. T. Zhang, and X. F. Han, Phys. Rev. B **93**, 054420 (2016).
[23] Y. J. Chen and S. Y. Huang, Phys. Rev. Lett. **117**, 247201 (2016).
[24] B. F. Miao, S. Y. Huang, D. Qu, and C. L. Chien, AIP Adv. **6**, 015018 (2016).
[25] J. Holanda, D. S. Maior, A. Azevedo, and S. M. Rezende, J. Magn. Magn. Mater. **432**, 507 (2017).
[26] H. Wang, C. Du, P. C. Hammel, and F. Yang, Phys. Rev. Lett. **113**, 097202 (2014).
[27] C. Hahn, G. de Loubens, V. V. Naletov, J. Ben Youssef, O. Klein, and M. Viret, Europhys. Lett. **108**, 57005 (2014).
[28] H. Wang, C. Du, P. C. Hammel, and F. Yang, Phys. Rev. B **91**, 220410(R) (2015).
[29] T. Moriyama, S. Takei, M. Nagata, Y. Yoshimura, N. Matsuzaki, T. Terashima, Y. Tserkovnyak, and T. Ono, Appl. Phys. Lett. **106**, 162406 (2015).
[30] W. Lin, K. Chen, S. Zhang, and C. L. Chien, Phys. Rev. Lett. **116**, 186601 (2016).
[31] A. Prakash, J. Brangham, F. Yang, and J. P. Heremans, Phys. Rev. B **94**, 014427 (2016).
[32] B. L. Zink, M. Manno, L. O'Brien, J. Lotze, M. Weiler, D. Bassett, S. J. Mason, S. T. B. Goennenwein, M. Johnson, and C. Leighton, Phys. Rev. B **93**, 184401 (2016).
[33] S. M. Rezende, R. L. Rodríguez-Suárez, and A. Azevedo, Phys. Rev. B **93**, 054412 (2016).
[34] S. M. Rezende, R. L. Rodríguez-Suárez, R. O. Cunha, A. R. Rodrigues, F. L. A. Machado, G. A. Fonseca Guerra, J. C. Lopez Ortiz, and A. Azevedo, Phys. Rev. B **89**, 014416 (2014).
[35] S. M. Rezende, R. L. Rodríguez-Suárez, J. C. López Ortiz, and A. Azevedo, J. Magn. Magn. Mater. **400**, 171 (2016).
[36] M. Hatami, G. E. W. Bauer, S. Takahashi, and S. Maekawa, Solid State Commun. **150**, 480 (2010).
[37] B. Scharf, A. Matos-Abiague, I. Zutic, and J. Fabian, Phys. Rev. B **85**, 085208 (2012).
[38] E. C. Stoner, Proc. R. Soc. London Sect. A **165**, 372 (1938).
[39] Y. Tserkovnyak, A. Brataas, and G. E. W. Bauer, Phys. Rev. B **66**, 224403 (2002).
[40] Y. Tserkovnyak, A. Brataas, G. E. W. Bauer, and B. I. Halperin, Rev. Mod. Phys. **77**, 1375 (2005).
[41] A. Slachter, F. L. Bakker, J.-P. Adam, and B. J. van Wees, Nat. Phys. **6**, 879 (2010).
[42] F. K. Dejene, J. Flipse, and B. J. van Wees, Phys. Rev. B **86**, 024436 (2012).
[43] K.-D. Lee *et al.*, Sci. Rep. **5**, 10249 (2015).
[44] C. Y. Ho, R. W. Powell, and P. Liley, *Thermal Conductivity of the Elements: A Comprehensive Review* (AIP, New York, 1978).
[45] C. Y. Ho, M. W. Ackerman, K. Y. Wu, S. G. Oh, and T. N. Havill, J. Phys. Chem. Ref. Data **7**, 959 (1978).
[46] M. Schreier *et al.*, J. Phys. D: Appl. Phys. **48**, 025001 (2015).
[47] J. Holanda, O. Alves Santos, R. L. Rodríguez-Suárez, A. Azevedo, and S. M. Rezende, Phys. Rev. B **95**, 134432 (2017).
[48] A. Kehlberger *et al.*, Phys. Rev. Lett. **115**, 096602 (2015).
[49] P. E. Mijnarends, S. Sahrakorpi, M. Lindroos, and A. Bansil, Phys. Rev. B **65**, 075106 (2002).
[50] R. M. Bozorth, *Ferromagnetism* (D. van Nostrand, New York, 1951).
[51] D. Y. Petrovykh, K. N. Altmann, H. Höchst, M. Laubscher, S. Maat, G. J. Mankey, and F. J. Himpsel, Appl. Phys. Lett. **73**, 3459 (1998).
[52] R. M. White, *Quantum Theory of Magnetism*, 3rd ed. (Springer, Berlin, 2007).
[53] T. R. McGuire and R. I. Potter, IEEE Trans Mag. **11**, 1018 (1975).